ISSN 1674-1056
http://cpb.iphy.ac.cn
http://iopscience.iop.org/cpb
中国物理 B
Chinese Physics
中国物理
Chinese Physics B

Rayleigh-Taylor instability at spherical interfaces of incompressible fluids

Hong-Yu Guo(郭宏宇), Li-Feng Wang(王立锋), Wen-Hua Ye(叶文华), Jun-Feng Wu(吴俊峰), Ying-Jun Li(李英骏), Wei-Yan Zhang(张维岩)
Citation: Chin. Phys. B . 2018, 27(2): 025206. **doi:** 10.1088/1674-1056/27/2/025206

Journal homepage: http://cpb.iphy.ac.cn; http://iopscience.iop.org/cpb

What follows is a list of articles you may be interested in

Rayleigh-Taylor instability of multi-fluid layers in cylindrical geometry

Hong-Yu Guo(郭宏宇), Li-Feng Wang(王立锋), Wen-Hua Ye(叶文华), Jun-Feng Wu(吴俊峰), Wei-Yan Zhang(张维岩)
Chin. Phys. B . 2017, 26(12): 125202. **doi:** 10.1088/1674-1056/26/12/125202

Magneto-Rayleigh–Taylor instability in compressible Z-pinch liner plasmas

Xue Yang(杨学), De-Long Xiao(肖德龙), Ning Ding(丁宁), Jie Liu(刘杰)
Chin. Phys. B . 2017, 26(7): 075202. **doi:** 10.1088/1674-1056/26/7/075202

Cylindrical effects in weakly nonlinear Rayleigh–Taylor instability

Liu Wan-Hai, Ma Wen-Fang, Wang Xu-Lin
Chin. Phys. B . 2015, 24(1): 015202. **doi:** 10.1088/1674-1056/24/1/015202

DD proton spectrum for diagnosing the areal density of imploded capsules on Shenguang Ⅲ prototype laser facility

Teng Jian, Zhang Tian-Kui, Wu Bo, Pu Yu-Dong, Hong Wei, Shan Lian-Qiang, Zhu Bin, He Wei-Hua, Lu Feng, Wen Xian-Lun, Zhou Wei-Min, Cao Lei-Feng, Jiang Shao-En, Gu Yu-Qiu
Chin. Phys. B . 2014, 23(7): 075207. **doi:** 10.1088/1674-1056/23/7/075207

Diagnostic technique for measuring fusion reaction rate for inertial confinement fusion experiments at Shen Guang-III prototype laser facility

Wang Feng, Peng Xiao-Shi, Kang Dong-Guo, Liu Shen-Ye, Xu Tao
Chin. Phys. B . 2013, 22(11): 115204. **doi:** 10.1088/1674-1056/22/11/115204

Rayleigh–Taylor instability at spherical interfaces of incompressible fluids*

Hong-Yu Guo(郭宏宇)[1,2], Li-Feng Wang(王立锋)[2,3], Wen-Hua Ye(叶文华)[2,3,†], Jun-Feng Wu(吴俊峰)[2], Ying-Jun Li(李英骏)[4,‡], and Wei-Yan Zhang(张维岩)[2,3]

[1] *Graduate School, China Academy of Engineering Physics, Beijing* 100088, *China*
[2] *Institute of Applied Physics and Computational Mathematics, Beijing* 100094, *China*
[3] *HEDPS, Center for Applied Physics and Technology, Peking University, Beijing* 100871, *China*
[4] *State Key Laboratory for Geomechanics and Deep Underground Engineering, China University of Mining and Technology, Beijing* 100083, *China*

(Received 26 September 2017; revised manuscript received 15 November 2017; published online 5 January 2018)

Rayleigh–Taylor instability (RTI) of three incompressible fluids with two interfaces in spherical geometry is derived analytically. The growth rate on the two interfaces and the perturbation feedthrough coefficients between two spherical interfaces are derived. For low-mode perturbation, the feedthrough effect from outer interface to inner interface is much more severe than the corresponding planar case, while the feedback from inner interface to the outer interface is smaller than that in planar geometry. The low-mode perturbations lead to the pronounced RTI growth on the inner interface of a spherical shell that are larger than the cylindrical and planar results. It is the low-mode perturbation that results in the difference between the RTI growth in spherical and cylindrical geometry. When the mode number of the perturbation is large enough, the results in cylindrical geometry are recovered.

Keywords: Rayleigh–Taylor instability, spherical geometry, inertial confinement fusion

PACS: 52.57.Fg, 47.20.Ma, 52.35.Py **DOI:** 10.1088/1674-1056/27/2/025206

1. Introduction

The Rayleigh–Taylor instability (RTI) occurs at a perturbed fluid interface where a light fluid supports another heavy fluid or accelerates a heavier one.[1,2] This instability plays a critical role in many areas, such as magnetized liner inertial fusion (MagLIF) experiment[3] and inertial confinement fusion (ICF) implosions.[4,5] In typically central ignition ICF implosion experiments, the spherical implosion target consisting of a high density ablator-fuel shell filled with a low density deuterium-tritium gas is irradiated directly by lasers or irradiated indirectly by x rays. During the acceleration stage, the dense shell is accelerated by the ablative plasmas, resulting in the instability that occurs on the outer interface of the shell. In the deceleration stage, the dense shell is decelerated by the central low density hot-spot, and the shell's inner interface is subject to the RTI. The RTI growth can cause the mixing of cold fuel with the hot-spot, leading to the large asymmetric deformation of a hot-spot, causing ICF implosion performance degradation and even resulting in ignition failure. So far, the Rayleigh–Taylor instability is still a critical issue in the ICF community.

The Rayleigh–Taylor instability has been investigated analytically,[6–18] numerically,[19–21] and experimentally[22,23] by many researchers. The classical RTI is first given by Rayleigh,[1] where two semi-infinite fluids are separated by a perturbed interface. The linear growth rate is obtained as $\gamma = \sqrt{Akg}$, where A is the Atwood number at the interface, k is the perturbed wave number, and g is the acceleration. Based on this classical configuration, RTI has been extensively studied by considering different factors like surface tension,[7] mass ablation,[9] density gradients,[10] and magnetic field,[11] etc. The linear growth of RTI for arbitrary stratified fluid layers is investigated by Mikaelian.[12] The interface coupling phenomenon is shown in Mikaelian's linear model.[13] The RTI growth in two finite-thickness fluids is studied in Ref. [8], it is found that the finite-thickness effect reduces the linear growth rate of RTI. The weakly nonlinear (WN) RTI in a finite-thickness slab is developed by Wang,[14] the feedthrough effect and the perturbation evolution are discussed in some detail. These analytical models mentioned above are limited to planar geometry. However, RTI always occurs in non-Cartesian geometries such as supernova explosions or ICF implosions. Yu[15] studied the RTI growth in cylindrical geometry (CG) for compressible fluid. The RTI growth at the spherical interface between viscous fluids is analyzed by Terrones.[16] The growth rate and the most unstable modes are illustrated analytically. Zhang[17] has developed a WN model for RTI growth at a single interface in spherical ge-

*Project supported by the National Natural Science Foundation of China (Grant Nos. 11275031, 11475034, 11575033, 11574390, and 11274026) and the National Basic Research Program of China (Grant Nos. 2013CB834100 and 2013CBA01504).

†Corresponding author. E-mail: ye_wenhua@iapcm.ac.cn
‡Corresponding author. E-mail: lyj@aphy.iphy.ac.cn

© 2018 Chinese Physical Society and IOP Publishing Ltd

ometry (SG). It is found the mode-coupling behavior in SG is different from that in CG. Recently, the RTI in multi-fluids is analyzed in CG.[18] The perturbation growth and the feedback effect between two cylindrical interfaces are discussed. In the spherical ICF implosion experiments, the source of perturbations on the inner interface of the imploded shell can be either initial perturbations due to the defects of the shell or the perturbations feedthrough from the outer interface. The feedthrough effect is a severe problem in ICF implosions that results in significant perturbation growth on the inner interface.[24,25] In this paper, we investigate the RTI growth of multi-fluid layers for the low-mode perturbations in SG.

This paper is organized as follows. Section 2 describes the theoretical model of the spherical RTI growth. The behavior of spherical RTI and the low-mode RTI growth are discussed in Section 3. Section 4 summarizes the major results and gives some conclusions.

2. Theoretical model

In this section, we will show the governing equations of the theoretical model. The coupling solutions for the RTI growth are also derived. The two-dimensional spherical coordinate system is introduced, where the r and θ are the radial direction and the polar direction, respectively. We consider three spherical fluid layers separated by an inner interface of radius R_1 and an outer interface of radius R_2 ($R_2 = R_1 + \Delta R$), where ΔR is the thickness of the middle layer. The three fluids are immersed in a gravitational field $\boldsymbol{g} = -g\boldsymbol{e}_r$ (i.e., during the deceleration stage of the ICF implosion). The two perturbed fluid interfaces can be expressed as $r(t,\theta) = R_1 + \eta_1(t,\theta)$ and $r(t,\theta) = R_2 + \eta_2(t,\theta)$, where the $\eta_1(t,\theta)$ and $\eta_2(t,\theta)$ are small perturbations at the inner and outer interfaces, respectively. In the following derivation, the physical quantities of the interior fluid ($0 < r < R_1$), the middle fluid ($R_1 < r < R_2$), and the exterior fluid ($R_2 < r < \infty$) will be denoted by the subscript "i", "m", and "e", respectively, unless otherwise stated. The governing equations for the present inviscid, irrotational, and incompressible fluids are

$$\frac{\partial \eta_1}{\partial t} + \frac{1}{r^2}\frac{\partial \eta_1}{\partial \theta}\frac{\partial \phi_\mathrm{i}}{\partial \theta} - \frac{\partial \phi_\mathrm{i}}{\partial r} = \frac{\partial \eta_1}{\partial t} + \frac{1}{r^2}\frac{\partial \eta_1}{\partial \theta}\frac{\partial \phi_\mathrm{m}}{\partial \theta} - \frac{\partial \phi_\mathrm{m}}{\partial r} = 0, \quad \text{at } r = R_1 + \eta_1, \tag{1}$$

$$\rho_\mathrm{i}\left\{\frac{\partial \phi_\mathrm{i}}{\partial t} + \frac{1}{2}\left(\frac{\partial \phi_\mathrm{i}}{\partial r}\right)^2 + \frac{1}{2r^2}\left(\frac{\partial \phi_\mathrm{i}}{\partial \theta}\right)^2 + gr\right\} - \rho_\mathrm{m}\left\{\frac{\partial \phi_\mathrm{m}}{\partial t} + \frac{1}{2}\left(\frac{\partial \phi_\mathrm{m}}{\partial r}\right)^2 + \frac{1}{2r^2}\left(\frac{\partial \phi_\mathrm{m}}{\partial \theta}\right)^2 + gr\right\} = f_1(t), \quad \text{at } r = R_1 + \eta_1, \tag{2}$$

$$\frac{\partial \eta_2}{\partial t} + \frac{1}{r^2}\frac{\partial \eta_2}{\partial \theta}\frac{\partial \phi_\mathrm{m}}{\partial \theta} - \frac{\partial \phi_\mathrm{m}}{\partial r} = \frac{\partial \eta_2}{\partial t} + \frac{1}{r^2}\frac{\partial \eta_2}{\partial \theta}\frac{\partial \phi_\mathrm{e}}{\partial \theta} - \frac{\partial \phi_\mathrm{e}}{\partial r} = 0, \quad \text{at } r = R_2 + \eta_2, \tag{3}$$

$$\rho_\mathrm{m}\left\{\frac{\partial \phi_\mathrm{m}}{\partial t} + \frac{1}{2}\left(\frac{\partial \phi_\mathrm{m}}{\partial r}\right)^2 + \frac{1}{2r^2}\left(\frac{\partial \phi_\mathrm{m}}{\partial \theta}\right)^2 + gr\right\} - \rho_\mathrm{e}\left\{\frac{\partial \phi_\mathrm{e}}{\partial t} + \frac{1}{2}\left(\frac{\partial \phi_\mathrm{e}}{\partial r}\right)^2 + \frac{1}{2r^2}\left(\frac{\partial \phi_\mathrm{e}}{\partial \theta}\right)^2 + gr\right\} = f_2(t), \quad \text{at } r = R_2 + \eta_2, \tag{4}$$

where ρ_i, ρ_m, and ρ_e are densities ($\rho_\mathrm{i} < \rho_\mathrm{m} > \rho_\mathrm{e}$). The ϕ_i, ϕ_m, and ϕ_e are the perturbed velocity potentials relating to the fluid velocities, $f_1(t)$ and $f_2(t)$ are arbitrary functions of time. Equations (1) and (3) represent the conditions that the normal velocity is continuous across the inner and outer interface, respectively. The Bernoulli equations (2) and (4) describe the pressure continuity condition across the inner and outer interface, respectively. Considering a single-mode spherical Legendre perturbation at two interfaces, the perturbation displacements $\eta_1(t,\theta)$ and $\eta_2(t,\theta)$ are expressed as

$$\eta_1(t,\theta) = \eta_\mathrm{i}(t)\,\mathrm{P}_l(\cos\theta), \tag{5}$$

$$\eta_2(t,\theta) = \eta_\mathrm{e}(t)\,\mathrm{P}_l(\cos\theta), \tag{6}$$

where $\mathrm{P}_l(\cos\theta)$ is the Legendre polynomial and l is the mode number. The η_i and η_e are the amplitudes of the perturbations.

The perturbed velocity $\phi_n(t,r,\theta)$ ($n = \mathrm{i},\mathrm{m}$, and e) can be written as

$$\phi_\mathrm{i}(t,r,\theta) = a_1(t) r^l\,\mathrm{P}_l(\cos\theta), \tag{7}$$

$$\phi_\mathrm{m}(t,r,\theta) = [a_2(t) r^l + a_3(t) r^{-(l+1)}]\,\mathrm{P}_l(\cos\theta), \tag{8}$$

$$\phi_\mathrm{e}(t,r,\theta) = a_4(t) r^{-(l+1)}\,\mathrm{P}_l(\cos\theta), \tag{9}$$

where $a_j(t)$ ($j = 1,2,3,4$) are the amplitudes of the corresponding perturbed velocity potentials. As can be seen in Eqs. (7)–(9), the perturbed velocity potentials $\phi_\mathrm{n}(t,r,\theta)$ have satisfied the Laplace equation $\nabla^2\phi_\mathrm{n} = 0$ and the boundary conditions $\nabla\phi_\mathrm{i}|_{r\to 0} = 0$ ($l \geq 2$) and $\nabla\phi_\mathrm{e}|_{r\to\infty} = 0$. We substitute Eqs. (5)–(9) into Eqs. (1)–(4) and expand the equations at the perturbed interfaces. Eliminating the time-dependent parameters $a_j(t)$, the governing equations for the evolutions of $\eta_\mathrm{i}(t)$ and $\eta_\mathrm{e}(t)$ are obtained as

$$\ddot{\eta}_\mathrm{i} - \frac{(1+\alpha_l)(1+A_1)\zeta^{-l+1}}{\chi_1 + 2A_1\zeta^{-2l-1}}\ddot{\eta}_\mathrm{e} - \frac{l}{R_1}\frac{2A_1 g\left(1-\zeta^{-2l-1}\right)}{\chi_1 + 2A_1\zeta^{-2l-1}}\eta_\mathrm{i} = 0, \tag{10}$$

$$\ddot{\eta}_\mathrm{e} - \frac{(1+\alpha_l)(1-A_2)\zeta^{-l-2}}{\chi_2 - 2\alpha_l A_2\zeta^{-2l-1}}\ddot{\eta}_\mathrm{i} - \frac{l}{R_2}\frac{2A_2 g\left(1-\zeta^{-2l-1}\right)}{\chi_2 - 2\alpha_l A_2\zeta^{-2l-1}}\eta_\mathrm{e} = 0, \tag{11}$$

where $\chi_1 = 1+\alpha_l - A_1/(1+l)$, $\chi_2 = 1+\alpha_l - A_2/(1+l)$, and $\alpha_l = l/(1+l)$. The $\zeta = R_2/R_1$ represents the ratio of the outer and the inner interface radius. The dot in the equations denotes the time derivative. As can be seen in Eqs. (10) and (11), the coupled second-order ordinary differential equations (ODEs) explicitly depend on the Legendre mode number l and Atwood numbers A_1 and A_2, where $A_1 = (\rho_m - \rho_i)/(\rho_m + \rho_i)$ and $A_2 = (\rho_e - \rho_m)/(\rho_e + \rho_m)$ are the Atwood numbers at the inner interface and the outer interface, respectively. In the limit of large mode number perturbation $l \gg 1$, the approximate expressions $\alpha_l \sim 1$, $\chi_1 \sim 2$, and $\chi_2 \sim 2$ are obtained. Then, the governing equations in SG are reduced to those in CG as follows:[18]

$$\ddot{\eta}_i - \frac{(1+A_1)\,\zeta^{-l+1}}{1+A_1\zeta^{-2l}}\ddot{\eta}_e - \frac{l}{R_1}\frac{A_1 g\left(1-\zeta^{-2l}\right)}{1+A_1\zeta^{-2l}}\eta_i = 0, \quad (12)$$

$$\ddot{\eta}_e - \frac{(1-A_2)\,\zeta^{-l+1}}{1-A_2\zeta^{-2l}}\ddot{\eta}_i - \frac{l}{R_2}\frac{A_2 g\left(1-\zeta^{-2l}\right)}{1-A_2\zeta^{-2l}}\eta_e = 0, \quad (13)$$

as can be seen above, the low-mode perturbation would result in the significant difference between SG and CG, which will be discussed in the following.

Considering that the two interfaces are initially perturbed with interface displacements, namely, $\eta_i(t=0) = \varepsilon_i$, $\dot{\eta}_i(t=0) = 0$, $\eta_e(t=0) = \varepsilon_e$, and $\dot{\eta}_e(t=0) = 0$. The ODEs for the amplitude of perturbations $\eta_i(t)$ and $\eta_e(t)$ are solved as

$$\eta_i(t) = \frac{1}{1-S_{12}S_{21}}\left[(\varepsilon_i - S_{21}\varepsilon_e)\cosh(\gamma_i t) + S_{21}(\varepsilon_e - S_{12}\varepsilon_i)\cosh(\gamma_e t)\right], \quad (14)$$

$$\eta_e(t) = \frac{1}{1-S_{12}S_{21}}\left[(\varepsilon_e - S_{12}\varepsilon_i)\cosh(\gamma_e t) + S_{12}(\varepsilon_i - S_{21}\varepsilon_e)\cosh(\gamma_i t)\right], \quad (15)$$

the perturbation growth on the two interfaces are coupled as illustrated in Eqs. (14) and (15). The coupling behaviors of the spherical RTI are similar to the results in cylindrical geometry.[18] However, the growth rates of spherical RTI and the feedback effects between two interfaces are different from that in CG. The coefficient S_{21} represents the feedback factor of the perturbation from the outer interface to the inner interface and the S_{12} denotes the feedback coefficient from the inner interface to the outer interface. The specific feedthrough coefficients S_{21} and S_{12} are

$$S_{21} = \frac{\tilde{\gamma}_e^2(1+\alpha_l)(1+A_1)\zeta^{-l+1}}{\tilde{\gamma}_e^2(\chi_1 + 2A_1\zeta^{-2l-1}) - 2A_1(1-\zeta^{-2l-1})}, \quad (16)$$

$$S_{12} = \frac{\tilde{\gamma}_i^2(1+\alpha_l)(1-A_2)\zeta^{-l-2}}{\tilde{\gamma}_i^2(\chi_2 - 2\alpha_l A_2\zeta^{-2l-1}) - 2A_2\zeta^{-1}(1-\zeta^{-2l-1})}, \quad (17)$$

as can be seen, the feedthrough coefficients are influenced by the shell thickness ΔR (represented by ζ), mode number l, and the Atwood numbers A_1 and A_2. The growth rates γ_i at the inner interface and γ_e at the outer interface are expressed as

$$\tilde{\gamma}_i^2 = \frac{\gamma_i^2}{gl/R_1} = \frac{s_2 + \sqrt{s_2^2 - 4s_1s_3}}{s_1}, \quad (18)$$

$$\tilde{\gamma}_e^2 = \frac{\gamma_e^2}{gl/R_1} = \frac{s_2 - \sqrt{s_2^2 - 4s_1s_3}}{s_1}, \quad (19)$$

the coefficients s_1, s_2, and s_3 are the functions of the Atwood numbers A_1,A_2, mode number l, and the ratio of radius ζ, which are written as

$$s_1 = \chi_1\chi_2 + 4\alpha_l\zeta^{-2l-1}A_1A_2, \quad (20)$$

$$s_2 = (1+\alpha_l)(A_1 + \zeta^{-1}A_2) - \left[(1-\alpha_l)(1+\zeta^{-1}) - 2(1-\alpha_l\zeta)\zeta^{-2(l+1)}\right]A_1A_2, \quad (21)$$

$$s_3 = \zeta^{-1}\left(1-\zeta^{-2l-1}\right)A_1A_2. \quad (22)$$

As illustrated in Mikaelian's planar results,[12] the growth rates are invariant under the condition $\rho_m \to \rho_i\rho_e/\rho_m$ (exchanging the value of A_1 and A_2). However, it is shown in Eqs. (18)–(22) that this symmetrical property is lost in spherical RTI. Considering short wavelength perturbations (the wavelength is much smaller than the shell thickness ΔR), we can obtain

$$\gamma_i(\Delta R \to \infty) = \sqrt{A_1\frac{l}{R_1}g\frac{2}{\chi_1}}, \quad (23)$$

$$\gamma_e(\Delta R \to \infty) = \sqrt{A_2\frac{l}{R_2}g\frac{2}{\chi_2}}, \quad (24)$$

which is identical to the linear results for RTI at a single spherical interface.[16,17] As can be seen, the two interfaces are decoupled for short wavelength perturbations. In the limit of long wavelength perturbations ($\Delta R \to 0$), the growth rates reduce to

$$\gamma(\Delta R \to 0) = \sqrt{\frac{(1+l)(\rho_e - \rho_i)}{(1+l)\rho_e + l\rho_i}\frac{l}{R}g}, \quad (25)$$

where $R_1 = R_2 \equiv R$. Equation (25) is the well-known linear growth rate of spherical RTI. When the mode number $l \to \infty$, the growth rate of the planar case is also recovered.[2]

It is interesting to note that the RTI growth in SG [Eqs. (14)–(22)] is approximately identical to that in CG[18] for large mode number perturbation ($l \gg 1$). For quite short wavelength perturbations compared to the radius, namely, $\tilde{\lambda} = 2\pi R_1/l \ll R_1$, the spherical results in this paper should reduce to that planar case. In the present work, we define the equivalent wavenumber $\tilde{k} = l/R_1$.[26] Considering a special case for

an infinity radius of R_1 and finite shell thickness ΔR, namely, $\Delta R \ll R_1 \to \infty$, then we have

$$\zeta^{-2l} = \left(\frac{R_2}{R_1}\right)^{-2l} = \left(1+\frac{\Delta R}{R_1}\right)^{-2l} \sim \mathrm{e}^{-2\tilde{k}\Delta R}, \quad (26)$$

$$\zeta^{-1} = \left(\frac{R_2}{R_1}\right)^{-1} = \left(1+\frac{\Delta R}{R_1}\right)^{-1} \sim 1, \quad (27)$$

the approximation in Eq. (26) is derived with the formula $\lim_{x\to\infty}(1+1/x)^x \sim e$. Mikaelian's planar results[12,13] are recovered with the approximations of Eqs. (26) and (27). That is to say, the behavior of RTI in the spherical case is similar to that in the planar case in the limit of large radius. Thus, the spherically convergence effect plays an important role for the low-mode RTI perturbations, which will be discussed below.

The above analytical results can be directly applied to the case in the presence of $\boldsymbol{g} = g\boldsymbol{e}_r$ by substituting $A_1 \to -A_1$, $A_2 \to -A_2$, and $g \to -g$, which will be of great interest in the acceleration stage of ICF implosion where the ablation surface is unstable and the hot-spot interface is stable.

3. Results and discussion

In this section, the growth rates of the RTI and the feedback effect between two interfaces in SG is discussed. The difference among the RTI growth in spherical, cylindrical, and planar geometry is also illustrated.

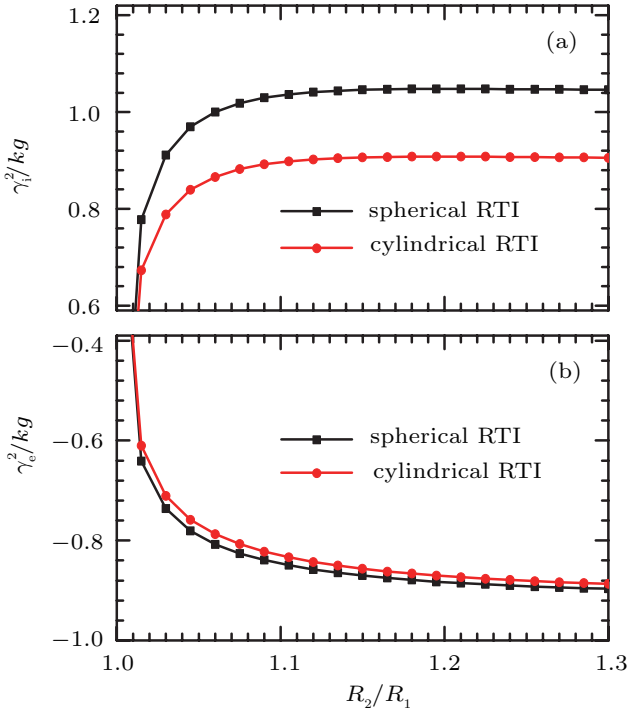


Fig. 1. (color online) Normalized growth rates $\gamma_i^2/\tilde{k}g$ (a) and $\gamma_e^2/\tilde{k}g$ (b) versus R_2/R_1 for mode number $l = 6$. The Atwood numbers are $A_1 = 0.9$ and $A_2 = -0.9$. The cylindrical results[18] are also displayed for comparison.

The dependencies of normalized growth rates $\gamma_i^2/\tilde{k}g$ and $\gamma_e^2/\tilde{k}g$ on R_2/R_1 are demonstrated in Fig. 1. For the case of $A_1 = 0.9$ and $A_2 = -0.9$, the inner interface of the middle shell is subject to the RTI. Thus, the value of $\gamma_i^2/\tilde{k}g$ is positive. With the increasing R_2/R_1, the $\gamma_i^2/\tilde{k}g$ increases gradually to a maximum value. The normalized growth rate $\gamma_e^2/\tilde{k}g$ is negative as the outer interface is stable. The absolute value of $\gamma_e^2/\tilde{k}g$ increases with increasing R_2/R_1, reaching to a maximum value at last. That means the thin shell effect (small R_2/R_1) will reduce the linear growth rate of RTI, which is consistent with our previous planar result.[8] The perturbations at two spherical interfaces are decoupled for large R_2/R_1, resulting in the individual growth rate for inner and outer interface, respectively. As can be seen in Fig. 1(a), the growth rate $\gamma_i^2/\tilde{k}g$ at the inner interface in SG is larger than that in the cylindrical case for fixed R_2/R_1. However, the growth rate $\gamma_e^2/\tilde{k}g$ at the outer interface in two geometries are approximately identical, which are shown in Fig. 1(b).

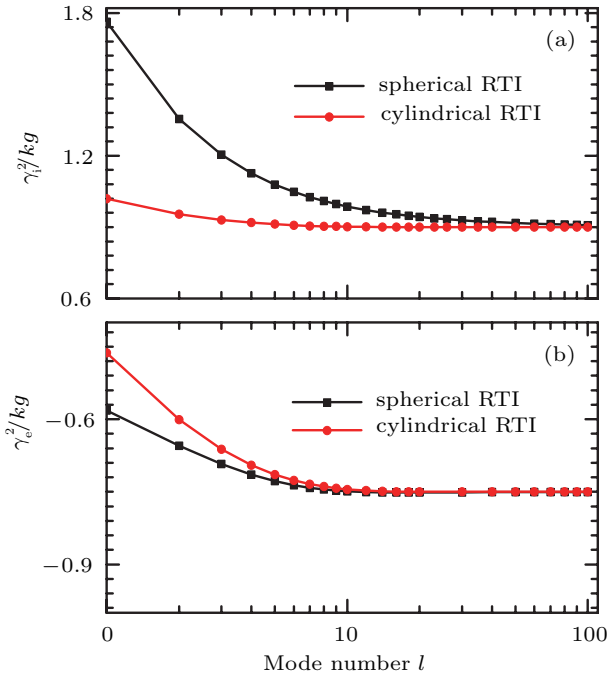


Fig. 2. (color online) The normalized growth rates $\gamma_i^2/\tilde{k}g$ (a) and $\gamma_e^2/\tilde{k}g$ (b) versus mode number l. The parameters are $A_1 = 0.9$, $A_2 = -0.9$, and $\zeta = 1.2$. The cylindrical results[18] are plotted together.

In Fig. 2, the effect of mode number l on the normalized growth rate $\gamma_i^2/\tilde{k}g$ and $\gamma_e^2/\tilde{k}g$ is displayed. The growth rate $\gamma_i^2/\tilde{k}g$ decreases with increasing l. The $\gamma_i^2/\tilde{k}g$ in spherical RTI is larger than that in the cylindrical case for low-mode number perturbation ($l < 20$), which is also shown in Fig. 1(a). The absolute value $\gamma_e^2/\tilde{k}g$ increases with increasing l and the spherical result is a little larger than the cylindrical result for $l < 5$. When l is large enough, the growth rates $\gamma_i^2/\tilde{k}g$ and $\gamma_e^2/\tilde{k}g$ in SG are completely equal to that in CG. That means the low-mode perturbation will cause much severe RTI growth in spherical implosions. This may be consistent with the recent simulation results of high-foot implosions on the National Ignition Facility (NIF)[27] where the low-mode perturbations at the inner interface have a large growth, leading to the large deformation of the hot-spot.

Figure 3 displays the relationship between the feedthrough coefficients S_{21}, S_{12}, and mode number l for different Atwood numbers. The coefficients S_{21} and S_{12} decrease to zero with increasing mode number l. That is to say, the two interfaces are decoupled for large mode number perturbation. It is because the perturbed wavelength is small when compared to the shell thickness for large l. The thick shell will lead to the enhanced feedthrough damping. The feedthrough coefficient S_{21} denotes the perturbation feedback from the outer interface to the inner interface that is influenced by A_2 at the outer interface. The S_{21} decreases quickly with the decreasing absolute value of A_2 for fixed l. When A_2 tends to -1.0, the approximation $S_{21} \sim (R_2/R_1)^{-l+1}$ is obtained that can be seen in Fig. 3(a). As shown in Fig. 3(b), the S_{12} (feedback from inner interface to outer interface) increases with increasing A_1 at the inner interface. When A_1 approaches to 1.0, we can find $S_{12} \sim (R_2/R_1)^{-l-2}$. Obviously, S_{21} is larger than S_{12} under the same conditions. However, the feedback coefficient between two interfaces of a planar slab is always e^{-kd}, where k is the wave number and d is the fluid thickness in the planar case.[7] It is the spherically convergence effect that leads to this difference between S_{21} and S_{12}.

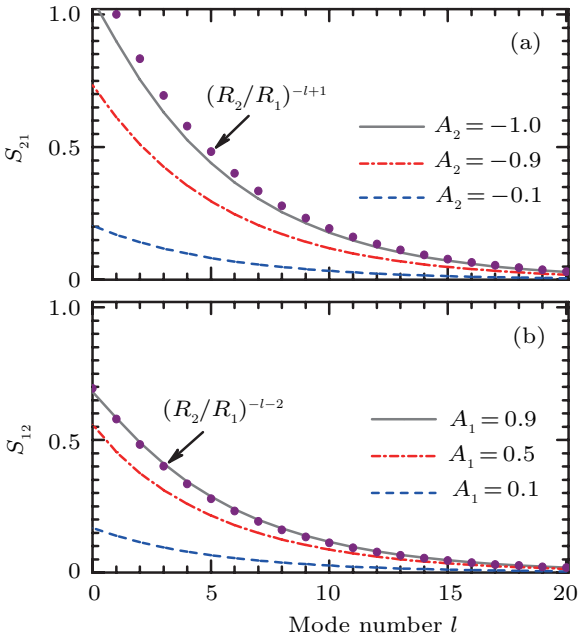


Fig. 3. (color online) The feedthrough coefficients S_{21} (a) and S_{12} (b) versus mode number l. The Atwood numbers are $A_1 = 0.8, A_2 = -0.1, -0.5, -1.0$ for S_{21} and $A_1 = 0.1, 0.5, 0.9$, $A_2 = -0.8$ for S_{12}, respectively. The radius ratio is $\zeta = 1.2$.

Figure 4 describes the dependence of coefficients S_{21} and S_{12} on normalized thickness $\tilde{k}\Delta R$ for various mode number l. The feedback effects become weak with the increasing $\tilde{k}\Delta R$, as the perturbations decay very fast when the shell becomes thick. The coefficient S_{21} is larger than the corresponding planar case for small l. When the mode number l is large enough ($l > 30$), Mikaelian's result is recovered.[13] As can be seen in Fig. 4(a), for the case of extremely low-mode perturbation ($l = 2$), the $S_{21} \sim 0.2$ in the spherical case is obtained for $\tilde{k}\Delta R = 3$, whereas the corresponding value is ~ 0 in the planar case. In other words, the planar interfaces are decoupled for $\tilde{k}\Delta R = 3$. However, the feedback effect from the outer interface to the inner interface still exists in SG for low-mode perturbation. Thus, it is worth pointing out that special attention must be given to the control of low-mode RTI growth for the ICF ignition target design. As displayed in Fig. 4(b), the feedthrough coefficient S_{12} is smaller than that in the planar case for small mode number perturbations.

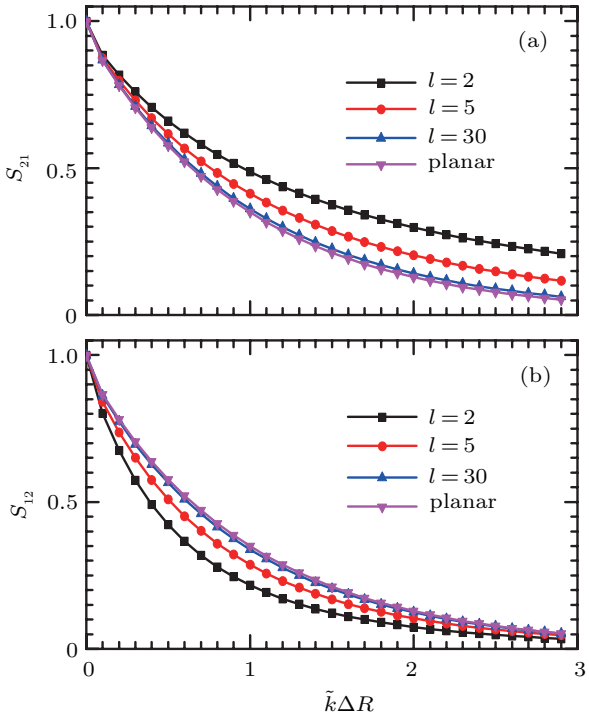


Fig. 4. (color online) The coefficients S_{21} (a) and S_{12} (b) versus the normalized shell thickness $\tilde{k}\Delta R$ for mode number $l = 2, 5, 30$. The Atwood numbers are $A_1 = 0.9$ and $A_2 = -0.9$. Mikaelian's planar result[13] is plotted for comparison.

Temporal evolutions of the normalized amplitudes of perturbations $\tilde{k}\eta_{\rm i}$ and $\tilde{k}\eta_{\rm e}$ initiated by inner interface perturbation alone and by outer interface perturbation alone are shown in Fig. 5. It can be clearly seen in Figs. 5(c) and 5(d), the phase of perturbations on the two interfaces initiated only by outer interface perturbation is shifted by π compared to that in Figs. 5(a) and 5(b) where only the inner interface is perturbed initially with the same amplitude. In Fig. 5(a), the amplitude $\tilde{k}\eta_{\rm i}$ in spherical RTI is larger than that in cylindrical and planar cases with the growing time, as the growth rate of spherical RTI is larger than the cylindrical and planar RTI for low-mode l. The amplitude $\tilde{k}\eta_{\rm e}$ on the outer interface in SG is a little larger than the other two cases, as the feedback coefficient S_{12} is smaller than that in the other two geometries, which is shown in Fig. 5(b). When the outer interface is initially perturbed alone, the RTI growth on the inner interface grows quickly with a negative phase due to the negative feedback effect that is displayed in Fig. 5(c). Although the inner interface is initially undisturbed, the amplitude of perturbation

on the inner interface still has a large growth especially for low-mode perturbation in SG. In Fig. 5(d), the perturbations on the outer interface oscillate at the beginning, and then grow rapidly with time because of the positive feedback effect from the inner interface. In short, the RTI growth in SG is very severe for low-mode perturbations. The high-foot implosions on the NIF indicate that the instability at the ablation surface has been effectively controlled but the low-mode perturbation growth at the inner interface is still very serious,[27] resulting in the severe deformation of hot-spot interface. Therefore, the low-mode perturbations of RTI must be strictly controlled in ICF implosions.

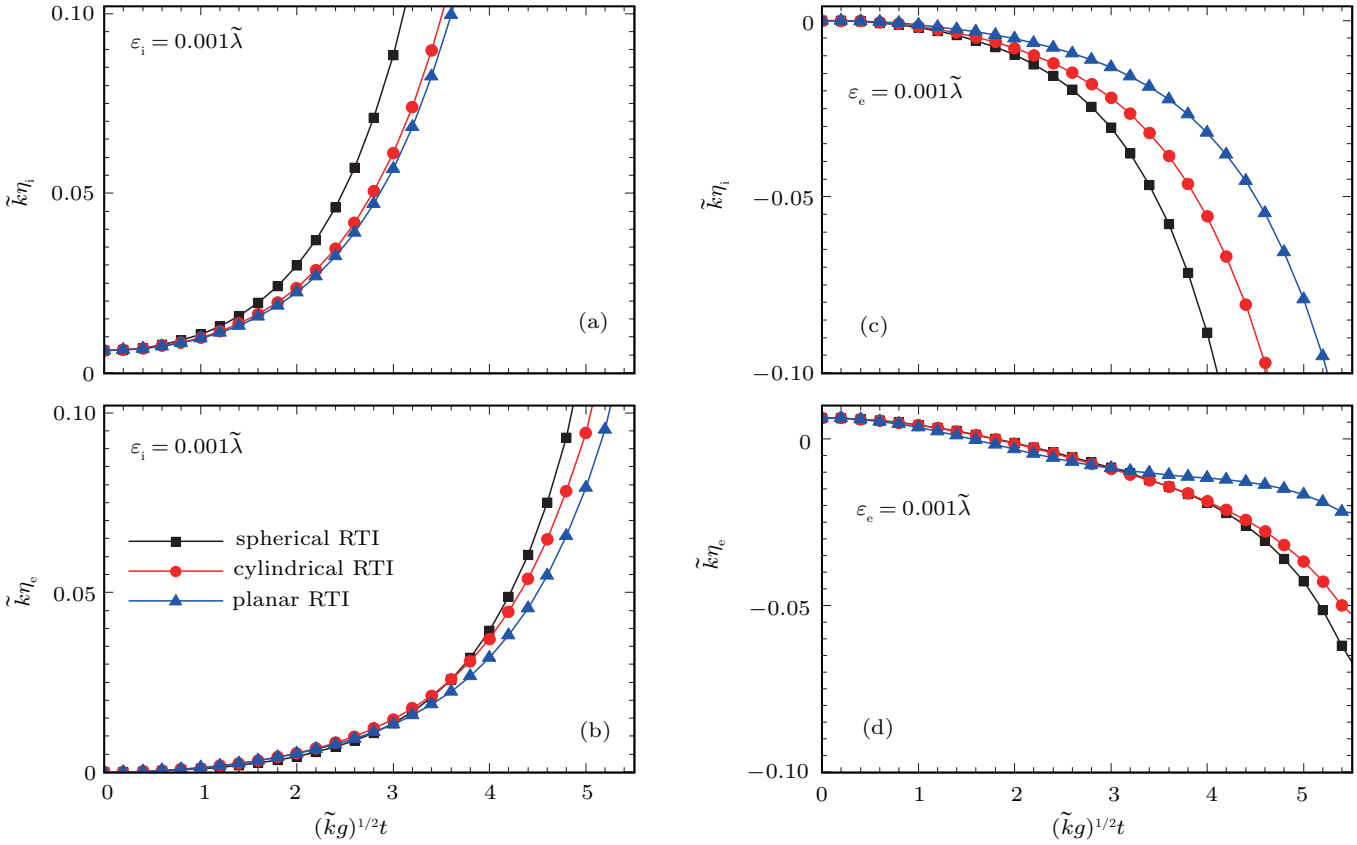


Fig. 5. (color online) The temporal evolutions of normalized amplitudes of perturbations $\tilde{k}\eta_i$ [panels (a) and (c)] and $\tilde{k}\eta_e$ [panels (b) and (d)] initiated by only the inner interface perturbation and by only the outer interface perturbation for normalized thickness $\tilde{k}\Delta R = 1.5$, respectively. Namely, $\varepsilon_i = 0.001\tilde{\lambda}$, $\varepsilon_e = 0$ for the left column [panels (a) and (b)] and $\varepsilon_i = 0$, $\varepsilon_e = 0.001\tilde{\lambda}$ for the right column [panels (c) and (d)]. The Atwood numbers are $A_1 = 0.9$ and $A_2 = -0.9$. The mode number is $l = 3$. The spherical, cylindrical, and planar results are plotted together.

4. Conclusion

In this research, the linear growth of RTI on two interfaces of three fluids in SG is investigated analytically. The two spherical interfaces are decoupled with increasing R_2/R_1. When the Atwood numbers $A_1 \to 1$ and $A_2 \to -1$, the feedthrough coefficient S_{21} from the outer interface to the inner interface is approximate to $\sim (R_2/R_1)^{-l+1}$ and S_{12} from the inner interface to the outer interface is approximately equal to $\sim (R_2/R_1)^{-l-2}$. We have compared the linear growth of the RTI in SG with that in cylindrical and planar cases. The growth rate in SG is larger than that in CG for low-mode perturbations. In the limit of $R_1 \to \infty$ and $\Delta R \ll R_1$, Mikaelian's planar result[13] is recovered. The perturbation growth is very severe in SG when compared to the corresponding cases in cylindrical and planar geometry, especially for the small mode number perturbations. For the low-mode perturbations, even though the initial perturbation is only imposed on the outer interface and the inner interface is kept unperturbed, there still exists a large RTI growth on the inner interface with a negative phase (compared to the initial perturbation) due to the negative feedback effect from the outer interface. In ICF implosions, the feedthrough effect can be a severe problem that contributes obvious perturbation growth to the inner interface.[4] Our model can be used to evaluate how much perturbations on the outer interface feed through to the inner interface. Furthermore, the present work could be valuable for verification of numerical codes.

Acknowledgment

The author (Hong-Yu Guo) wishes to thank Prof. Xian-Tu He for his useful discussion and help.

References

[1] Rayleigh L 1883 *Proc. London Math. Soc.* **14** 170
[2] Taylor G 1950 *Proc. R. Soc. Lond. A* **201** 192

[3] Awe T J, McBride R D, Jennings C A, Lamppa D C, Martin M R, Rovang D C, Sinars D B, Slutz S A, Owen A C, Tomlinson K, Gomez M R, Hansen S B, Herrmann M C, McKenney J L, Robertson G K, Rochau G A, Savage M E, Schroen D G and Stygar W A 2014 *Phys. Plasmas* **21** 056303
[4] Lindl J D, Amendt P, Berger R L, Glendinning S G, Glenzer S H, Haan S W, Kauffman R L, Landen O L and Suter L J 2004 *Phys. Plasmas* **11** 339
[5] Wang L F, Ye W H, He X T, Wu J F, Fan Z F, Xue C, Guo H Y, Miao W Y, Yuan Y T, Dong J Q, Jia G, Zhang J, Li Y J, Liu J, Wang M, Ding Y K and Zhang W Y 2017 *Sci. China-Phys. Mech. Astron.* **60** 055201
[6] Guo H Y, Yu X J, Wang L F, Ye W H, Wu J F and Li Y J 2014 *Chin. Phys. Lett.* **31** 044702
[7] Guo H Y, Wang L F, Ye W H, Wu J F and Zhang W Y 2017 *Chin. Phys. Lett.* **34** 045201
[8] Guo H Y, Wang L F, Ye W H, Wu J F and Zhang W Y 2017 *Chin. Phys. Lett.* **34** 075201
[9] Garnier J and Masse L 2005 *Phys. Plasmas* **12** 062707
[10] Wang L F, Ye W H and Li Y J 2010 *Phys. Plasmas* **17** 042103
[11] Yang B L, Wang L F, Ye W H and Xue C 2011 *Phys. Plasmas* **18** 072111
[12] Mikaelian K O 1982 *Phys. Rev. A* **26** 2140
[13] Mikaelian K O 1983 *Phys. Rev. A* **28** 1637
[14] Wang L F, Guo H Y, Wu J F, Ye W H, Liu J, Zhang W Y and He X T 2014 *Phys. Plasmas* **21** 122710
[15] Yu H D and Livescu D 2008 *Phys. Fluids* **20** 104103
[16] Terrones G and Carrara M D 2015 *Phys. Fluids* **27** 054105
[17] Zhang J, Wang L F, Ye W H, Wu J F, Guo H Y, Zhang W Y and He X T 2017 *Phys. Plasmas* **24** 062703
[18] Guo H Y, Wang L F, Ye W H, Wu J F and Zhang W Y 2017 *Chin. Phys. B* **26** 125202
[19] Ye W H, Zhang W Y and He X T 2002 *Phys. Rev. E* **65** 057401
[20] Wang L F, Ye W H, He X T, Zhang W Y, Sheng Z M and Yu M Y 2012 *Phys. Plasmas* **19** 100701
[21] Yan R, Betti R, Sanz J, Aluie H, Liu B and Frank A 2016 *Phys. Plasmas* **23** 022701
[22] Hsing W W, Barnes C W, Beck J B, Hoffman N M, Galmiche D, Richard A, Edwards J, Graham P, Rothman S and Thomas B 1997 *Phys. Plasmas* **4** 1832
[23] Wilkinson J P and Jacobs J W 2007 *Phys. Fluids* **19** 124102
[24] Simakov A N, Wilson D C, Yi S A, Kline J L, Clark D S, Milovich J L, Salmonson J D and Batha S H 2014 *Phys. Plasmas* **21** 022701
[25] Yi S A, Simakov A N, Wilson D C, Olson R E, Kline J L, Clark D S, Hammel B A, Milovich J L, Salmonson J D, Kozioziemski B J and Batha S H 2014 *Phys. Plasmas* **21** 092701
[26] Haan S W 1989 *Phys. Rev. A* **39** 5812
[27] Dittrich T R, Hurricane O A, Callahan D A, Dewald E L, Doppner T, Hinkel D E, Berzak Hopkins L F, LePape S, Ma T, Milovich J, Moreno J C, Patel P K, Park H S, Remington B A and Salmonson J 2014 *Phys. Rev. Lett.* **112** 055002